Fire Safety Journal 152 (2025) 104346

Contents lists available at ScienceDirect

Fire Safety Journal

journal homepage: www.elsevier.com/locate/firesaf

Large-scale compartment fires to develop a self-extinction design framework for mass timber-Part 2: Results, analysis and design implications

Felix Wiesner [a,**], Hangyu Xu [b], David Lange [b], Vinny Gupta [c,d], Ian Pope [e], José L. Torero [f], Juan P. Hidalgo [b,*]

[a] The University of British Columbia, Canada
[b] The University of Queensland, School of Civil Engineering, Australia
[c] The University of Sydney, Department of Aerospace, Mechanical and Mechatronics Engineering, Australia
[d] University of Waterloo, Department of Mechanical and Mechatronics Engineering, Canada
[e] DBI – The Danish Institute of Fire and Security Technology, Denmark
[f] University College London, Department of Civil, Environmental and Geomatic Engineering, UK

ARTICLE INFO

Keywords:
Performance-based design
Compartment fires
Heat transfer
Protection of wood
Large-scale
Cross-laminated timber
Mass timber
Char fall-off

ABSTRACT

This paper seeks to provide key fundamental knowledge underpinning the use of self-extinction principles as part of a design framework for buildings with engineered mass timber structures. The results from six compartment fire experiments in a cross-laminated timber (CLT) enclosure with different ratios of exposed timber are presented and analyzed to establish the effects of timber exposure on the dynamics of a fire and on the potential of the fire to self-extinguish. The results show the relevance of four key parameters that need to be considered concurrently when assessing self-extinction in mass timber compartments: (a) the characteristic time for burnout of the movable fuel load, (b) the characteristic time for the occurrence of char fall-off, (c) the characteristic time for the occurrence of encapsulation failure, and (d) the heat exchange within the compartment after consumption of the moveable fuel. Self-extinction was attained only when the characteristic time for the occurrence of char fall-off was longer than the characteristic time for burn-out and the heat exchange after burn-out resulted in a heat flux below a well-defined threshold. The position of the exposed timber surfaces affected the magnitude of the threshold heat flux. If the characteristic time for burn-out was greater than the characteristic time for encapsulation failure, self-extinction was not observed to occur.

1. Introduction

Engineered timber is increasingly being used as the main structural material for larger or more innovative building types. This is mostly driven by sustainability [1] and expedited construction schedules [2]. Wood is combustible and fire safety thus has been a key design aspect for engineered timber buildings. If the structural timber is allowed to ignite, the requirement to achieve self-extinction is critical to fire safety [3]. If the structural timber does not self-extinguish then the structure cannot fulfill the necessary requirement to be able to withstand burn-out, and the total loss of the building can be envisioned. This is generally an unacceptable outcome for any complex, and particularly tall, buildings.

This paper aims to establish the fundamental principles underpinning a design framework for self-extinction of engineered mass timber. This work follows a literature review (Part 1) [4] of the existing body of work, the conceptual background for self-extinction, and a detailed description of the methodology for a series of six large-scale compartment fire experiments that were designed to isolate the key phenomena of importance. The fundamentals of self-extinction have been defined [5–8]. If the timber surface energy balance falls below a critical value, flaming self-extinction will occur. This must ensue before materialization of effects that increase heat flux to the wood, like loss of encapsulation or char fall-off.

Char oxidation can continue in the absence of a flame, this condition corresponds to smouldering, but needs to be clearly differentiated from the self-extinction process described above, which corresponds to the extinction of a gas phase flame. While ongoing heat release from smouldering is a real and possible fire safety hazard to timber

* Corresponding author.
** Corresponding author.
E-mail addresses: felix.wiesner@ubc.ca (F. Wiesner), j.hidalgo@uq.edu.au (J.P. Hidalgo).

https://doi.org/10.1016/j.firesaf.2025.104346
Received 5 April 2024; Received in revised form 18 January 2025; Accepted 21 January 2025
Available online 27 January 2025

compartments [9–12], the analysis and discussion herein is limited to flaming combustion and its cessation. Therefore, herein, self-extinction is defined as cessation of flaming from combustible surfaces that form part of the structure and burnout is defined as the flameout of the moveable fuel load in the compartment. Burnout will occur in all compartments, while self-extinction can only occur in compartments with exposed timber elements.

At any given time, the heat balance at the char surface is dominated by the compartment fire dynamics. Thus, it is essential to understand the relationship between ignition and burning of the mass timber, the burning history of the movable fuel load, the transient decay of the fire as the movable fuel load is consumed and the compartment geometry and characteristics that define heat exchange towards the compartment surfaces.

In this context, the state of the art review [4], identified four key considerations necessary to evaluate the potential for self-extinction as: (1) the thermal feedback between burning timber surfaces; (2) the occurrence of char fall-off, which has the potential to expose unburnt timber, thereby contributing to increase the heat released and thermal feedback; (3) encapsulation failure, which also exposes additional timber to participate in the compartment fire, thus increasing the fuel load and overall heat release rate; and (4) the burning duration of the movable fuel load. Six compartment fire experiments that were designed to explicitly tie these considerations to extinction conditions are presented here.

2. Methodology

An overview of the experiments and their relation to the self-extinction criteria described in the previous section is shown in Fig. 1. The timber exposure, expressed as a ratio of the exposed area (A_e) to the total area of compartment surfaces (A_T), excluding the opening, was varied from 0 (no surfaces exposed) to 0.35 (one wall and the ceiling exposed) and 0.52 (two walls and the ceiling exposed). Fig. 2 illustrates different exposure conditions. The influence of different timber exposure on the gas phase compartment fire dynamics has been extracted from earlier work [13,14]. The duration of the test was defined by either the time at which burnout and/or self-extinction was deemed to have occurred or the time at which manual extinguishing was performed.

The burning duration of the moveable fuel load (4) is the key defining condition for self-extinction as it drives the thermal penetration depths into the plasterboard and timber and is key to establishing the temporal evolution of the thermal field. Thus, a key aim of these tests was to carefully control moveable fuel load (Fig. 1). Two different fuel types were used to assess their respective influence on self-extinction mechanisms: a kerosene pool fire or a wood crib. This was necessary because the fuel has a controlling effect on the overall compartment fire dynamics, and therefore, the temporal evolution of the thermal boundary condition of the plasterboard and timber [15–18].

Detailed descriptions of the experimental methodology were provided in Ref. [4]. Herein, only key details are reiterated. The compartments were built from radiata pine cross-laminated timber (CLT) with a thickness of 125 mm, comprising a lamination set-up of 45-35-45 mm, and a measured mean bulk density of 485 kg/m^3. The mean moisture content of CLT throughout the testing programme varied between 10 and 14 %, as measured with a handheld moisture meter and validated from sacrificial samples with oven drying. The adhesive used was Loctite HB S, a one component polyurethane adhesive. The internal dimensions of the compartment were 3.15 m × 3.15 m × 2.7 m, with a single opening measuring 0.85 m × 2.1 m. These compartment dimensions were not intended to replicate real compartments, but to create a space that allowed experiments to elucidate key conditions that were defined in Ref. [4]. The available ventilation was deliberately kept low and consistent to guarantee maximum temperatures and homogeneity of the interior temperature fields.

Key instrumentation comprised: a custom-built buoyancy calorimeter measuring the total heat release rate based on the burned effluent gases [19]; thermocouples (TCs) measuring gas and solid-phase (in-depth) temperatures; thin-skin calorimeters (TSCs) to measure total incident heat flux on both the inert and timber walls [20]; bi-directional velocity probes (BDPs) measuring local gas flow velocities within the compartment and at the opening; gas analysers measuring oxygen, carbon dioxide and carbon monoxide concentrations [19]; and platform scales to measure the mass loss rate of the fuel. Internal locations of TCs, TSCs and BDPs are shown in Appendix A.

Ignition of the pool fires was with a rag at the end of a metal pole,

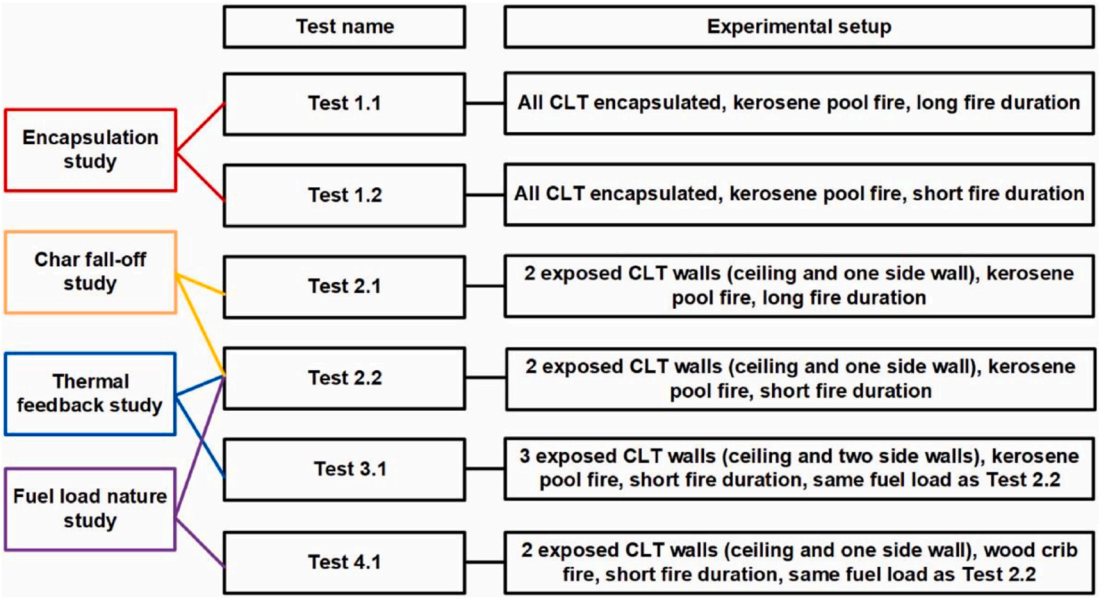

Fig. 1. Overview of the experimental conditions tested that highlights how changes in set-up target outcome parameters [4]. Tests 1.1 and 1.2 serve as a benchmark representing a non-combustible compartment and enabling to establish failure characteristics of the encapsulation. Tests 2.1 and 2.2 explore the duration of the movable fuel load and its impact on char fall-off and thermal feedback, Test 3.1 adds the effect of more exposed surface and finally Test 4.1. alters the thermal exposure by including the fire decay of a timber crib.

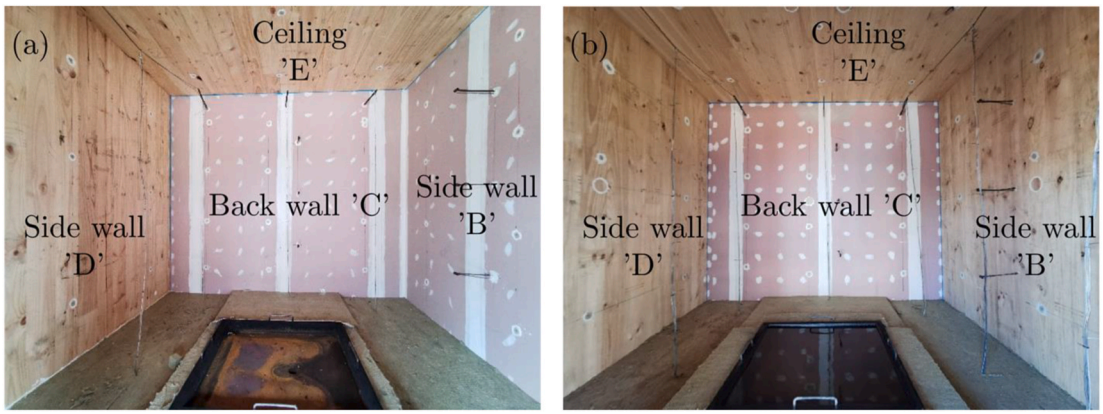

Fig. 2. Images showing interior of timber compartments with kerosene pool before fire. Subfigure a) shows the Ceiling 'E' and Side wall 'D' exposed while Back wall 'C' and Side wall 'B' are covered by gypsum board. Subfigure b) shows the Ceiling 'E', Side wall 'B', and Side wall 'D' exposed while Back wall 'C' is covered by gypsum board.

soaked with kerosene, that was ignited with a blowtorch outside the compartment and then temporarily placed on the surface of the kerosene nearest the door. For the wood crib, ignition was via four metal trays of 0.94 m length, each filled with 0.42 L kerosene, that were placed within the second, fourth, seventh and ninth gaps out of the ten gaps at the base of the wood crib. These trays were ignited with a blowtorch sequentially.

The burning duration of the kerosene pool fire was controlled by an external fuel supply system, similar to the system previously used by Tondini and Franssen [21] and adopted for compartment fires by Gorska et al. [22]. The projected floor area of the wood crib was identical to the pool fire (1 m × 1 m), with the fuel load density of the crib adjusted by controlling the total number of layers of sticks. The fuel load density was selected to match the total heat released by the kerosene pool fire where no char fall-off occurred and self-extinction was achieved. The burning rate of kerosene is higher than that of timber and therefore the fire duration will be shorter in the case of the kerosene pool.

The flame heights for the kerosene pool fires were approximately half the compartment height just after ignition, however, due to the fast formation of a deep smoke layer the flame height was soon reduced to a narrow area of 10–20 cm above the fuel surface. For the wood crib the flame heights of the wood crib were higher, with limited impingement on the ceiling and the exposed timber wall.

No significant leakages other than the intended ventilation opening were observed, except for Test 2.1, late in the test, when the compartment was breached. Localised smouldering remained after flaming suppression for all tests with the exception of Test 1.1 ($A_e/A_T = 0$, short duration pool fire). Post-flaming extinction smouldering phenomena was not the subject of this study so these pockets of smouldering were actively extinguished at the end of the tests.

The occurrence of self-extinction is discussed on the basis of three characteristic times, the characteristic times for burnout of the fuel load (t_{bo}), of char fall-off occurrence ($t_{f,c}$) and of encapsulation failure ($t_{f,e}$). Herein, char fall-off is defined as the physical separation of pieces of char and their movement to the compartment floor under the influence of gravity. The temporal evolution of the thermal feedback within the compartment after the movable fuel burnout was also monitored.

Before flashover, the rates of heat transfer to the timber structure and the encapsulation were considered negligible compared to the rates during the post-flashover stage. Therefore, all plots in the following section are aligned to start at flashover. This is done to allow comparison between tests that exhibited different times to flashover (defined as the uppermost gas-phase thermocouples reaching a mean temperature of 600 °C).

To compare the charring rates in each experiment, the charring rate was calculated 15 min after flashover based on the interpolated position of the 300 °C isotherm at each TC cluster. After tests 2.2, 3.1, and 4.1, the exposed CLT panels were cut up to allow visual measurement of the final char depths in the vicinity of the thermocouple clusters – five on each panel – as defined in Ref. [4]. This was not done for Test 2.1, since the almost total charring of all exposed CLT layers, including complete burn-through in some areas, meant that measurement of a char layer profile would not have been meaningful.

3. Results and analysis

The main characteristics and outcomes of the tests in each of the parameter studies are summarised in Table 1.

3.1. General observations and self-extinction

3.1.1. Burning duration of the movable fuel load

Failure to self-extinguish occurs when modes such as encapsulation failure ($t_{f,e}$) or char fall-off ($t_{f,c}$) occur, which are processes that are dependent on the time-history of the thermal boundary condition on the encapsulation layer or timber. Therefore, the characteristic time for the burnout of the movable fuel load (t_{bo}) is a key parameter in the assessment of self-extinction occurrence. The burnout time is governed by the total fuel load (expressed in kg or MJ) and the fuel burning rate (expressed in kg/s or MJ/s, respectively). The moveable fuel load is a controllable parameter (generally dependent on the building occupancy), while the fuel burning rate in a compartment fire is controlled by contextual variables (e.g. air vitiation), thermal feedback from the compartment, and the fuel mass transfer number of all combustible materials [16].

The baseline tests 1.1 and 1.2 are used to establish a relationship between the burnout duration and the fuel load per unit floor area for this specific compartment and type of fuel (kerosene pool fire). Tests 1.1 and 1.2 were both fully encapsulated, i.e., had no initially exposed timber, and differed only in how long the continuous fuel supply was provided to the pool fire. Fig. 3 shows the amount of fuel consumed as a function of fire duration and per unit area of the floor.

The quantification and control of the fuel load was undertaken, (1) to highlight the capability of the pool fire system to establish a fuel load with different characteristics, and (2) to quantify the total fuel load so as to benchmark the fuel load against possible fuel loads that could arise in other experimental studies or as part of engineering calculations. For instance, the average load for offices and dwellings according to Eurocode 1 [23] are shown as horizontal lines (420 and 780 MJ/m^2, respectively). It is shown that the expected office fuel load was exceeded after approximately 25 min, while the test duration was not sufficient to match the expected dwelling fuel load. Applying linear extrapolation of the data, and thus ignoring the acceleration from plasterboard

Table 1
Summary of main test parameters and outcomes.

Study	Test ID	Exposure ratio (A_e/A_T)	Moveable fuel load (MJ, MJ/m^2)	Duration until end of test (min)	End of test	Charring rates[a] & final char depths[b] (mm/min, mm)	Outcome
Encapsulation	1.1	0	6439, 649	38	Manually extinguished	N/A, N/A	Failure of encapsulation
	1.2	0	1310, 132	14	Burnout	N/A, N/A	No encapsulation failure
Char fall-off	2.1	0.35	7855, 792	60	Manually extinguished	1.06–1.76, N/A[c]	Char fall-off & compartmentation breach
	2.2	0.35	3156, 318	31	Flaming self-extinction	0.84–1.49, 21 - 36 (50)[d]	Flaming self-extinction
Thermal feedback	3.1	0.52	3004, 303	41	Manually extinguished	1.11–2.39, 48–83	Char fall-off & encapsulation failure
Fuel type (wood crib)	4.1	0.35	3106, 313	52	Manually extinguished	1.11–2.53, 47–91	Char fall-off, encapsulation failure, & compartmentation breach

[a] Estimated from thermocouple measurements and interpolation of the 300 °C isotherm at 15 min after flashover.
[b] Representative range from visual measurements after the test in five locations on each exposed CLT panel.
[c] Representative final char profiles could not be established for Test 2.1. In some places, the entire CLT panel had burned through.
[d] Maximum values in brackets observed in an isolated location, e.g., near cracks or gaps between wood pieces.

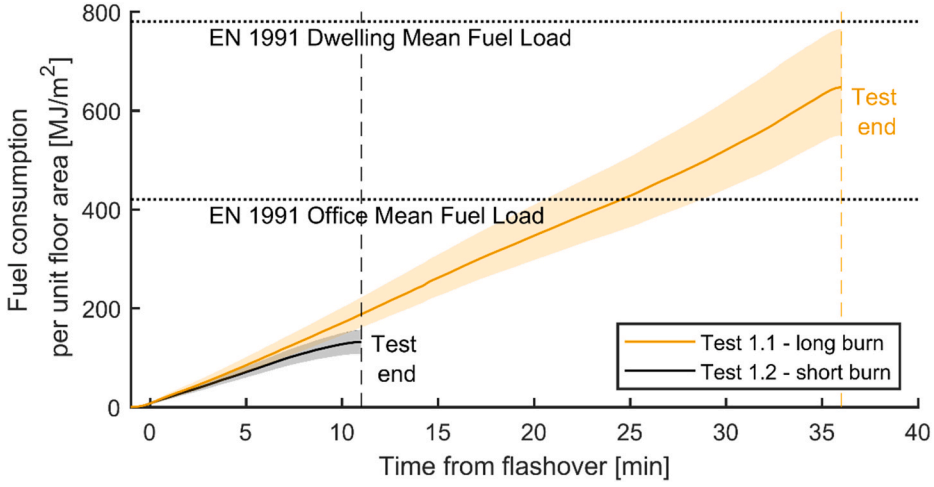

Fig. 3. Cumulative fuel consumption per unit area from kerosene pool fire against time from ignition for tests 1.1 and 1.2. Fuel consumption was calculated from HRR measurements which were calculated from the range of possible measurements from the velocity measurements and gas concentrations within the doorway. By estimating the possible magnitude of the errors associated to the HRR a range of possible values was calculated and is presented as shaded area.

heating/failure, it can be approximated that the dwelling fuel load would have been attained after approximately 48 min of burning. After the fuel flow to the pool was closes ('fuel off') the pool fires did not immediately extinguish as remaining kerosene continued to burn.

Slight differences in the slope, and thus the kerosene HRR, for the two tests can potentially be attributed to a fault with the water-cooling system for the pan in Test 1.2 (short), which may have caused small quantities of water to leak into the kerosene; this was rectified for all subsequent tests.

3.1.2. Heat release rates

The total heat release rates, as measured from the buoyancy calorimeter, for all six experiments are shown in Fig. 4. After flashover, the HRR increased rapidly followed by a fully developed stage where the HRR changes slowly. Finally, a rapid decay stage follows the onset of self-extinction/fire suppression.

During the fully-developed stage, the contribution of exposed timber is shown to have approximately doubled the HRR from the kerosene pool fire, compared to tests where all timber was encapsulated (1.1 and 1.2). With a peak HRR of 6.5 MW, the highest HRR was measured for Test 3.1, which had three exposed timber surfaces (Walls B, D and the Ceiling E), compared to tests 2.1, 2.2, and 4.1, which all had their Ceiling E and Wall D exposed. The median total HRR during the fully

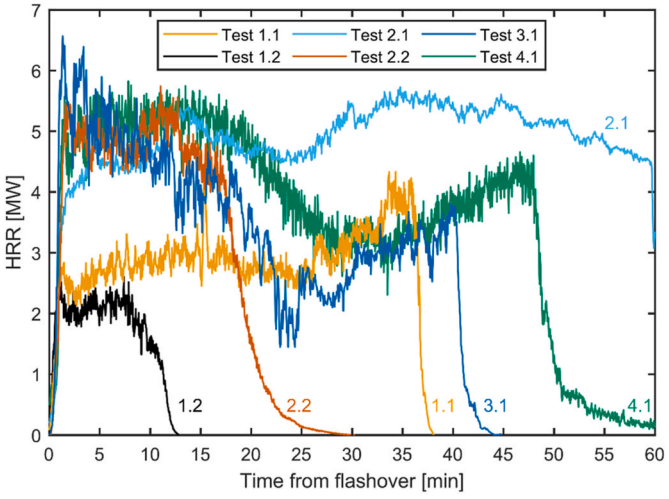

Fig. 4. Total heat release rate measured from the point of flashover for all tests reported herein.

developed stage of the burning was found to be 2.8, 2.1, 4.8, 4.8, 4.9, and 5.2 MW for tests 1.1, 1.2, 2.1, 2.2, 3.1 and 4.1, respectively.

Complete flaming self-extinction of the burning timber in the compartment was achieved for only Test 2.2 ($A_e/A_T = 0.35$, short duration kerosene pool fire). The other tests involving exposed timber required manual intervention with water jets to force extinction. A brief summary description of the failure modes inhibiting flaming self-extinction are as follows:

- Test 1.1 ($A_e/A_T = 0$, long duration pool fire), failure induced by encapsulation failure: This test was designed to identify the encapsulation failure for a completely encapsulated compartment. While no timber was originally exposed, the gradually increasing encapsulation failure led to exposure of timber surfaces from a large fraction of the compartment.
- Test 2.1 ($A_e/A_T = 0.35$, long duration pool fire), failure primarily induced by char fall-off: This test was designed to induce failure so the conditions for failure could be quantified, enabling a selection of permissible fuel loads for subsequent tests. Test 2.1 exhibited char fall-off, as has been described in prior papers [3,24]. The char fall-off exposed virgin timber, thereby increasing the effective fuel load and simultaneously the timber burning rate. The additional char on the floor effectively increased the thermal radiation received by all the burning timber surfaces in the compartment.
- Test 3.1 ($A_e/A_T = 0.52$, short duration pool fire), failure induced by excessive thermal feedback: This test had three exposed timber surfaces (ceiling, and the two side walls), which provided sufficient thermal feedback to each other for continuous burning after the kerosene fuel had burnt out. This feedback was a combination of radiative feedback between the burning surfaces, and the high heat release provided by the exposed timber that continued to burn. This was sufficient to sustain a deep layer of hot combusting gases in the upper half of the compartment. The high thermal feedback was then subsequently increased by char fall-off, for the same reasons as in Test 2.1.
- Test 4.1 ($A_e/A_T = 0.35$, wood crib), failures primarily induced by prolonged burning duration: The wood crib, which had an equivalent fuel load to the kerosene pool in Test 2.2 and Test 3.1, was used as the moveable fuel load in this test. This resulted in a longer burning duration (including the effect of prolonged radiant heat flux from the collapsed smouldering wood crib) and as a result self-extinction did not occur before char fall-off, which caused a gradual increase in HRR and ultimately the test had to be stopped.

3.1.3. *Surface heat fluxes*

The measured spatial median heat flux measurements on different surfaces in the compartment are shown for tests 1.2, 2.2, 3.1 and 4.1 in Fig. 5. For all tests shown, an increase in measured heat flux could be observed following flashover. The panel with the door opening (Surface A), recorded the lowest total heat flux exposures, which can be explained by the effect of cold air entrainment through the door.

The highest heat fluxes were measured for Test 3.1 after the movable fuel load burnout, as in this test three timber surfaces were exposed resulting in the highest heat release within the compartment. Test 4.1 (wood crib burn) shows a noticeably greater demarcation of heat fluxes compared to the other pool fire tests. The heat fluxes received on encapsulated surfaces A, B, and C (see Fig. 2 were relatively uniform compared to the kerosene pool fires, suggesting that the resulting gas phase thermal conditions were more spatially homogenous. For tests, 3.1, and 4.1, which both exhibited char fall-off, the heat fluxes increased after char fall-off occurred. For each test, heat fluxes measured on exposed timber surfaces prior to char fall-off attained similar values

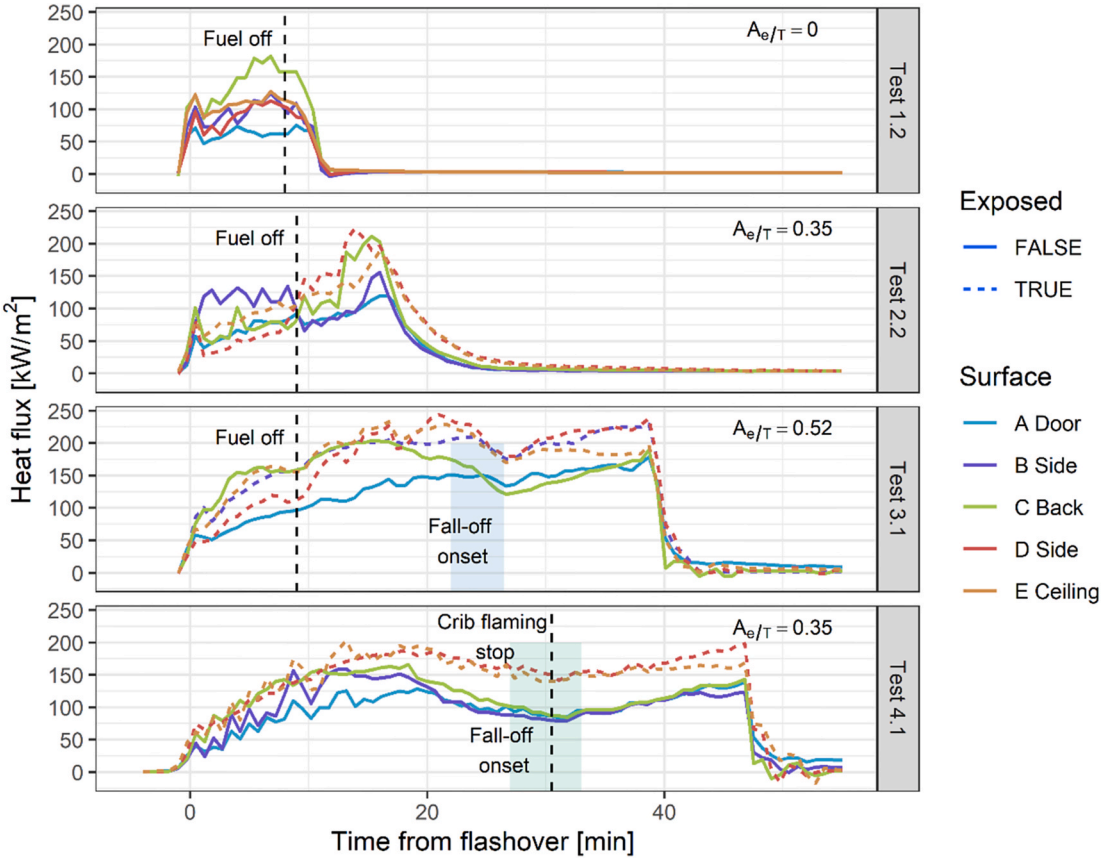

Fig. 5. Heat flux measurements from thin skin calorimeters in different tests, for different compartment surfaces. The plotted values are spatial medians across each surface.

until the end of the tests; at this point exposed walls recorded larger heat fluxes than the exposed ceiling.

3.2. Failure of encapsulation

Encapsulation failure ($t_{f,e}$) has been described as the insulation and integrity failure of passive fire protection, which is commonly used to prevent the onset of pyrolysis of the timber surface. This failure time is dependent on the evolution of the incident heat flux, the fire protection material, its thickness and arrangement (i.e. number of boards and mechanical fastener system and spacing). The use of plasterboard is a common feature in fire safety strategies, not only for mass engineered timber but also for stick frame construction, utilising either wood or steel studs. Within the fire resistance framework, the performance of different encapsulation systems has been extensively tested globally and formalised into codified guidance. Research into encapsulation performance on different substrates in natural fires [25] is also available. In this section, we do not aim to assess the performance of an encapsulation system. Instead, we analyse the characteristic time for the occurrence of encapsulation failure in the context of the time to burn-out, to emphasize the role of failure of encapsulation as a function of the burning of the movable fuel load and in relationship to the failure of the fire to self-extinguish.

For all other tests herein, two layers of plasterboard, were used, with the exception of Test 2.1 ($A_e/A_T = 0.35$, long duration pool fire). For Test 2.1 an additional layer of Rockwool was placed between the two plasterboard layers, to attempt preventing encapsulation failure and thus to ensure a focus on the char fall-off study.

Failure of the encapsulation was studied by initially running a long burn time (Test 1.1), and identifying through post-processing of the data the encapsulation failure time, $t_{f,e}$. Test 1.2 had a deliberately short burning duration so that the encapsulation will not fail and the fire ended without any intervention after the external kerosene supply was removed and the fuel had burnt out.

The total and internal HRR are shown in Fig. 6 a) and b), respectively. The total HRR was determined from flow through the buoyancy calorimeter while internal HRR was determined from flow and gas concentrations measured at the compartment opening. The measured HRR for Test 1.2 plateaued at approximately 2–2.5 MW and started to decrease 7 min after flashover when the kerosene supply to the pool was closed.

The solid-phase temperatures at the interface of plasterboard and encapsulated timber for the three instrumented walls and the ceiling are shown in Fig. 7 a) and b) for the short and long fully-encapsulated tests, respectively. A clear distinction in median panel temperatures can be identified both for the short and long test. In both cases, the back wall (Wall C) shows the fastest median temperature increase. Under complete encapsulation, comparatively larger inflow velocities were measured resulting in a pronounced plume tilting effect [14], resulting in direct flame impingement onto the back wall. The momentum-driven flows effectively enhance the total heat transfer to the back wall (Wall C). This results in both higher and spatially uniform gas temperatures and total heat fluxes. The fluid mechanics and resulting heat transfer processes are extensively reported on by Pope et al. [14].

For the longer test (Test 1.1), the plasterboard began to fail (insulation failure) at around 25 min. Parts of the outer encapsulation layer were visually observed to crack and fall after 16–18 min, while portions of the inner layer started to fall off after 27 min. The first observation of complete plasterboard dehydration at the timber interface in Test 1.1 was measured after 23.2 min. This exposes parts of the virgin timber to the fire, causing an increase in the total heat release rate due to the pyrolysis of the exposed timber. The temperatures at the interface also started to increase rapidly – coinciding with the observations of fall-off from the inner plasterboard layer.

Chemically endothermic dehydration reactions inside the porous plasterboard result in loss of mechanical properties and therefore define the onset of failure of the plasterboard [26]. Therefore, the effectiveness of the plasterboard can be gauged from the overall proportion of thermocouples at the CLT-plasterboard interface that remain below a selected critical temperature threshold. The temperature distributions shown in Fig. 7 indicate a strong plateau around 100 °C which corresponds to the endothermic dehydration process. The failure of plasterboard is characterized by the sudden increase of temperature beyond the endothermic plateau.

Fig. 8, shows the proportion of all 100 solid-phase TCs in Test 1.1 that exceed either 95, 105, or 300 °C. The first two were chosen as ± 5 % of the boiling point of water at 1 atm and represent the plateau observed in Fig. 7. The third threshold of 300 °C is chosen as the commonly utilised temperature to indicate the onset of significant pyrolysis from wood to char [27,28]. Fig. 8 shows that the time for the first significant increase in exceedance of the 95 °C lower bound was approximately 12 min after flashover. The time for attainment of the 105 °C threshold was approximately 24 min after flashover and charring of the timber at the timber/plasterboard interface occurred approximately 26 min after flashover and coincided with the observation of first plasterboard fall-off.

Given that the increase in number of thermocouples at the plasterboard-timber interface exceeding 105 °C correlates well with the

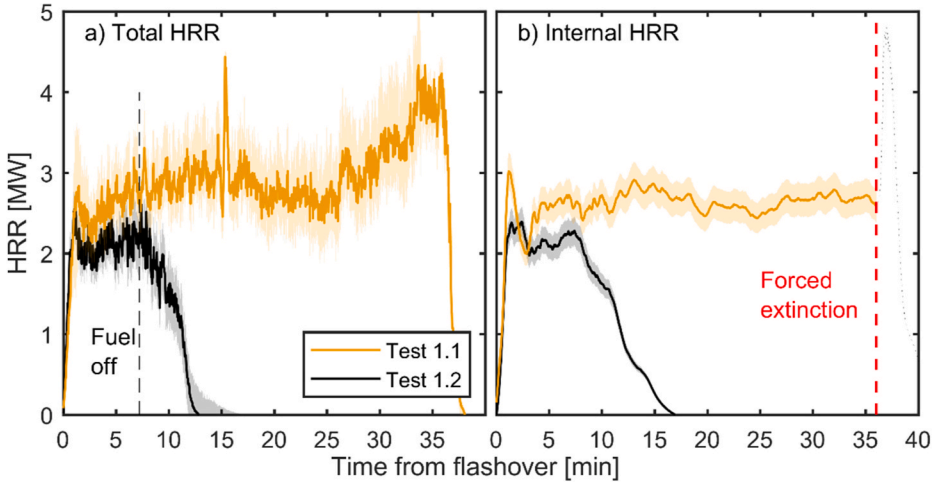

Fig. 6. Heat release rate measurements for fully encapsulated tests 1.1 and 1.2 showing a) total HRR as measured from external buoyancy calorimeter and b) internal HRR of kerosene fuel pan as determined from calorimetry gas species and flow at the compartment opening.

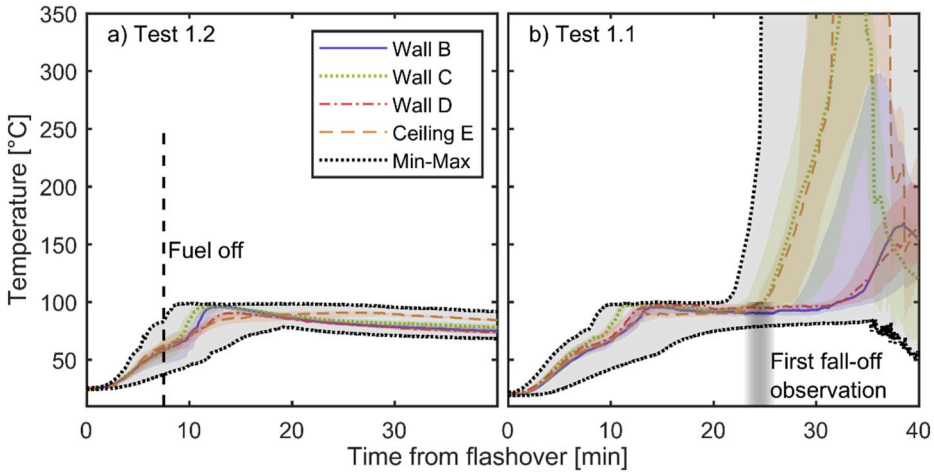

Fig. 7. Temperatures at the CLT-plasterboard interface for ceiling (E), left (D), right (B), and back wall (C) in Test 1.2 (a) and Test 1.1 (b). The black dotted lines indicate the maximum and minimum temperature reached in all panels. The shaded areas show interquartile ranges of temperature measurements for each individual panel.

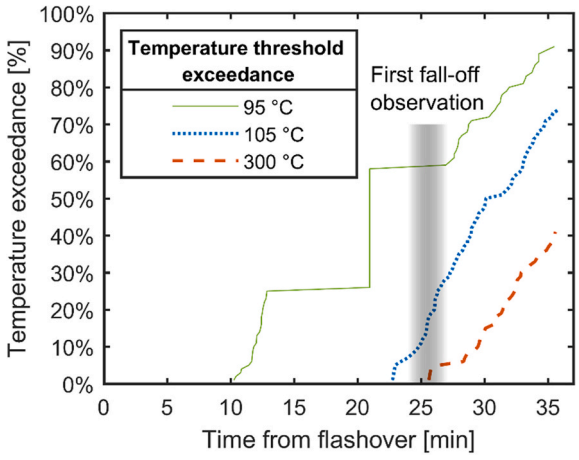

Fig. 8. Proportion of exceedance of selected temperature thresholds for all thermocouples at the CLT-plasterboard interface during Test 1.2.

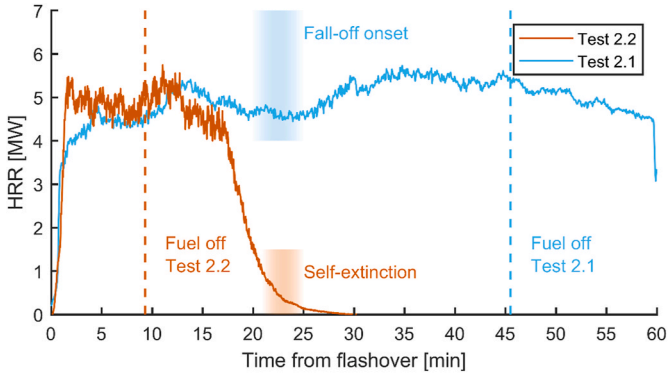

Fig. 9. Total heat release rate measurements for a compartment with two exposed timber surfaces and either a short (Test 2.2) or long kerosene pool burning duration (Test 2.1).

increase in the total HRR from the compartment fire the temperature exceedance criterion of 105 °C was deemed appropriate to define plasterboard failure and the participation of previously unexposed timber in the compartment fire. This threshold is applicable only for this installation and should not be used as a threshold that universally defines plasterboard encapsulation.

3.3. Char fall-off study

Char fall-off has been identified as a key failure mode for self-extinction in laminated timber compartments [3,29–31]. In this study, tests 2.1 and 2.2 replicate identical conditions, apart from the fuel load (burnout time), which was increased in Test 2.1 to extend burning and observe char fall-off and measure the critical thermal conditions before and during its occurrence. The measured total HRR for these tests are shown in Fig. 9.

For Test 2.2, the kerosene fuel supply was closed 9 min after flashover, leading to burnout of the remaining kerosene in the pan until all 'moveable fuel' was consumed. No char fall-off was observed, and both the measured total HRR and the temperatures in the compartment dropped, with flaming self-extinction observed to progress from the bottom of the exposed wall (Wall D) upwards until all major flaming stopped without external intervention. This observation is consistent with the measured heat fluxes, which were greater in the upper-regions of the compartment after the moveable fuel was consumed [13]. After flaming self-extinction inside the compartment was attained, smouldering combustion was observed to continue in localised "hotspots".

For Test 2.1 the fuel supply was maintained for 46 min after flashover. Char fall-off was observed from approximately 20 min after flashover, resulting in an increasing fire size, HRR and a longer external flame through the opening. After 60 min, flames had breached the entire section of CLT in localised regions in the exposed wall and ceiling of the compartment, resulting in external flaming that necessitated immediate suppression.

A key consideration for char fall-off and its relevance to fire safety design is the solid-phase temperatures near the glue lines. As the thermal conditions throughout the compartment are not homogeneous [13,14], the thermal penetration also varies correspondingly with the spatial distribution of energy. To consolidate this data, two temperature thresholds of the solid phase at the glue lines are considered as time of exceedance: (1) 300 °C due to its association with significant pyrolysis. This temperature is also sometimes used as a criterion for char fall-off to occur [5]. However, weakening of the adhesive capacity has been reported at lower temperatures [32–36], therefore, (2) herein a lower bound threshold temperature of 100 °C is also considered, based on its association with moisture movement and drying processes.

The increase of temperatures at the first glue line, which is the first location where significant char fall occurs, is shown for the exposed

timber surfaces for Test 2.1 and Test 2.2 in Fig. 10 a) and b), respectively. These allow a comparison of the effects of heating duration on the temperature at the glue line contextualized by the observation of char fall-off.

For Test 2.2 with shorter imposed burning duration, the glue line temperatures continued to increase after fuel shut off. However, the median temperatures increased only slightly and for approximately 20 min before plateauing at 100 °C followed by slow cooling. Comparatively, in Test 2.1 (long burn), the temperature-rise accelerated rapidly. While there was a plateau at 100 °C, it was comparatively short.

The visual observation of the onset of char fall-off closely aligned with rapid increases in the hottest temperatures at the glue line. The sudden rise is expected as the char fall-off enabled the increase of heat transfer (or even direct flame exposure) to the thermocouple. The median plateau for 100 °C lasted for less than 2 min. The subsequent median increase from 100 °C to 300 °C took less than 5 min (4.8 min). This indicates that times to critical temperature for prevention of fall-off lie within relatively narrow ranges.

3.3.1. Exceedance

Similar to the assessment for plasterboard failure, the probability of exceedance of selected temperature thresholds at the first glue line of the CLT is shown in Fig. 11. These temperatures correspond to exposed timber in Test 2.1. The first observations of char fall-off coincided with the first exceedance of glue line temperatures of 95 °C. The time delay between the attainment of overall glue line temperature exceedance of 95 °C and 105 °C is almost non-existent for ceiling and wall and only delayed by a few minutes for the temperature exceedance of 300 °C, particularly when comparing the delays to those of the encapsulation study tests (Test 1.1 and Test 1.2) in Fig. 7.

Observations confirm that the onset of char fall-off was a very localized process, thus these systemic approaches based on critical conditions, such as a critical temperature, do not provide sufficient insight to characterize char fall-off. The large bounds of maximum and minimum glue-line temperatures in Fig. 10 (b) are evidence that the onset of char fall-off is highly localised. Characteristic in-depth heating times are very long, therefore, temporal variations in the gas phase cannot be responsible for the observed variability. Nevertheless, the spatial variation of in-depth heating is beyond the scope of this paper.

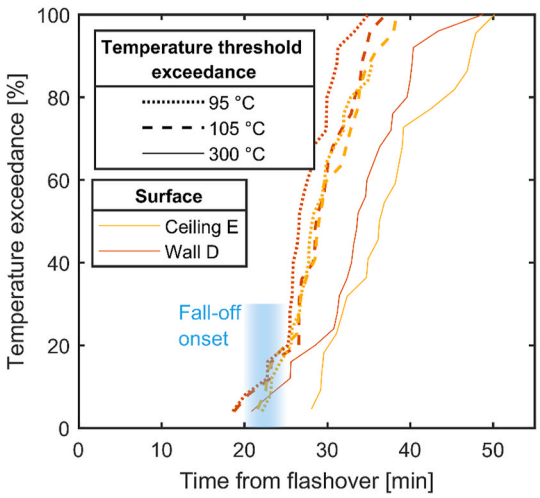

Fig. 11. Exceedance of selected temperature thresholds for all thermocouples at the first CLT glue line during Test 2.1 for exposed surfaces.

3.4. Thermal feedback study

Thermal feedback refers to the heat transfer between the burning exposed timber surfaces and the smoke layer caused by the burning timber. If the net heat flux at the char-pyrolysis interface remains above a critical value, pyrolysis of the timber will continue to sustain combustion and therefore the timber will continue to burn at a rate proportional to the net heat flux [4,37]. Re-radiation from the burning timber surfaces, the flames established over the timber surface, and the smoke layer are critical factors controlling the incident heat flux over each exposed surface. Therefore, both A_e/A_T and the geometric placement of the timber surfaces are key to the quantification of thermal feedback and the potential attainment of flaming self-extinction. This experimental series studied the role of thermal feedback at a large-scale by varying A_e/A_T through Test 2.2 ($A_e/A_T = 0.35$) and Test 3.1 ($A_e/A_T = 0.52$). Both tests were run with short duration pool fires, with the total fuel consumption in each of these tests kept as consistent as possible and quantified by combining the mass loss measured by the scale beneath the pool fire tray and the flow meter connected to the fuel tank. The two pool fires in Test 2.2 and Test 3.1 released heat of 3156 MJ and 3004 MJ, respectively, equivalent to 73 kg and 70 kg of kerosene.

The time-evolution of the HRR for both tests is shown in Fig. 12, including indicators for critical events. The graphs show that, as already established, Test 2.2 achieved flaming self-extinction before any char fall-off. At flashover, Test 3.1 was measured to have a slightly higher

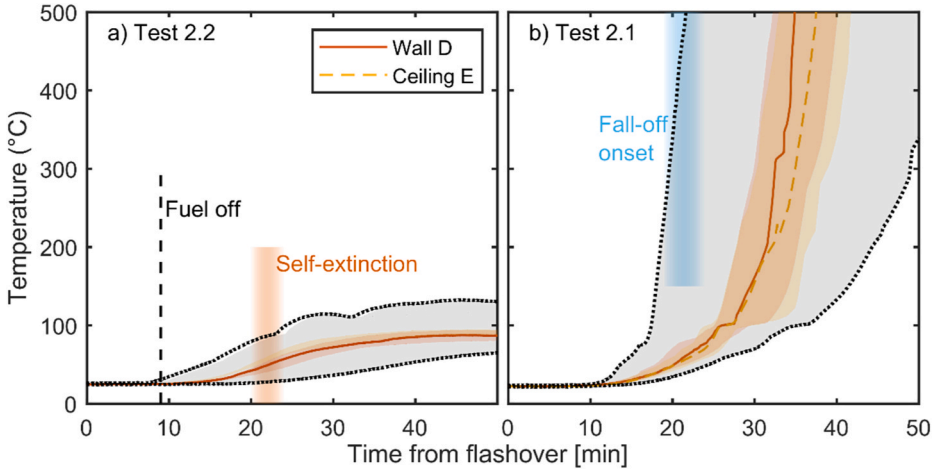

Fig. 10. Temperatures at the first CLT glue line for exposed ceiling E, and exposed side wall D in (a) Test 2.2 and (b) Test 2.1. The black dotted lines indicate the maximum and minimum temperature reached in these panels. The shaded areas show interquartile ranges of temperature measurements for each individual panel. The slightly faster onset of maximum temperatures in Test 2.1 compared to Test 2.2 are attributed to individual thermocouples, rather than systematically different behaviour; this is evidenced by the similar onset of temperature increase for the spatial median across wall/ceiling in both tests.

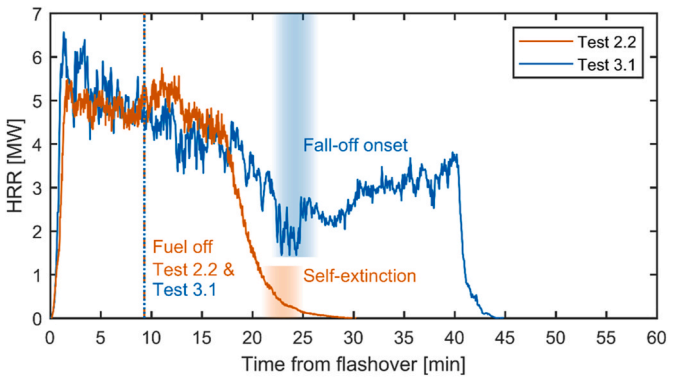

Fig. 12. Heat release rate measurements for tests with quasi equal fuel load and either two (Test 2.2) or three (Test 3.1) exposed timber surfaces.

total HRR than Test 2.2 due to the heat release contribution from the additional timber surface that had already ignited. A peak HRR of 6.6 MW was measured in Test 3.1, which is approximately 1.1 MW (20 %) larger than the one measured for Test 2.2 with two exposed surfaces. For a wall area of 8.37 m^2 exposed timber this translates to a peak heat release rate per unit area (HRRPUA) of 131.4 kW/m^2 from the additional exposed wall. This value is within the expected contribution range for cellulosic fuels [38].

The influence of the increased heat feedback is also evident in the slower decay of the HRR after the kerosene burned out. After approximately 21 min, just before self-extinction was observed for Test 2.2, the HRR for Test 3.1 reached an inflection point (at about 2 MW) which coincided with the observation of onset of char fall-off and the subsequent increase in the HRR. After the char fall-off exposed fresh timber, a continued increase in HRR was measured with char fall-off progressing up to a point where the floor was completely covered with fallen char pieces after around 34 min. This continued until the HRR was measured as approximately 3.8 MW. At this point self-extinction was deemed to not be achievable and the fire was extinguished through application of a water jet. The process of self-extinction for Test 2.2 is contrasted against the ongoing burning of the three surfaces in Test 3.1 in Fig. 13 a) and b), respectively. In both cases the kerosene pool fire has burnt out, resulting in enhanced visibility from the cleaner burning timber.

In comparison to Hadden et al. [3], who had reported a test, denoted 'Gamma', with three-sided exposure in a similarly sized compartment, we measured a peak HRR of 3.8 MW after burnout of kerosene, which is very similar to the steady state HRR reported by Hadden et al. of approx. 3.5 MW. However, a decay down to 2 MW was observed here after the kerosene fuel had burnt out, while Hadden et al. never reported a reduction in HRR below 3.5 MW. This can be attributed to the different thicknesses of lamellae. Hadden et al. used CLT with an outer layer thickness of 20 mm, compared to 45 mm herein. A thicker layer delays the time for the glue line to heat up and thus, for Hadden et al., the onset of fall-off coincided with the burnout of the fuel load, while here a thicker char layer was established as the kerosene fuel burnt out allowing for a greater decay in the burning rate before fall-off occurred.

The surface incident heat flux conditions for flaming self-extinction are examined in detail in Fig. 14 a), and b), which show the TSC derived heat flux values for the time period where self-extinction occurred in Test 2.2, for exposed Wall D and Ceiling E, respectively. The shown heat flux values are from individual TSCs on each exposed surface and thus show higher variance than the spatial medians shown in Fig. 5. A critical value of 40 kW/m^2 is superimposed alongside the visually observed time period over which self-extinction was recorded; the value of 40 kW/m^2 was chosen based on bench-scale findings of self-extinction by Cuevas et al. [39], who recorded this value as an upper limit for upwards facing CLT in a Fire Propagation Apparatus. The time period over which self-extinction occurred is longer for Wall D, for which self-extinction was observed to start at floor level and to transit along the wall. For the ceiling self-extinction began near the unexposed Wall B and moved towards the shared exposed edge with Wall D, which was the location where self-extinction occurred last.

For Wall D, the onset of self-extinction coincides closely with the self-extinction threshold of 40 kW/m^2, which also aligns with recent findings by Hopkin et al. [40], however, for the ceiling, self-extinction begins at heat fluxes markedly above 40 kW/m^2, at approximately 70 kW/m^2 – this may be due to limited availability of oxygen near the ceiling, compared to the wall.

The energy balance for self-extinction (and lack thereof) may also be considered at the pyrolysis region, as was defined in Ref. [4]. Herein this is considered from the temperature gradient at the char-timber interface and is calculated at multiple positions of high in-depth temperature thermocouple clusters. The thermocouple readings from known depths were used to calculate the position of the char-timber interface for each time-step using a smoothing spline [41] and a 300 °C [27] temperature threshold. The temperature gradient was then calculated from a differentiation of a 3rd degree polynomial fit at the previously located 300 °C isotherm, i.e. the timber-char interface. The resulting heat flux from the char to the pyrolyzing timber was then calculated as shown in Equation (1) as the product of the temperature gradient (at the char side of the pyrolysis front (x_p^-)) and the thermal conductivity of the char (k_c), which was assumed as 0.097 W/mK at 300 °C [42].

$$-k_c \frac{\partial T}{\partial x}\bigg|_{x=x_p^-} = \dot{q}''_{c\to p} - k_w \frac{\partial T}{\partial x}\bigg|_{x=x_p^+} \tag{1}$$

The second term corresponding to in-depth heat losses was found by Emberley et al. [7] not to rapidly attain a constant value, so for the purposes of this analysis it will not be considered and $\dot{q}''_{c\to p}$ will be established only in terms of the gradient in the char. The heat flux values ($-k_c \frac{\partial T}{\partial x}\big|_{x=x_p^-} \propto \dot{q}''_{c\to p}$) for the exposed ceiling are shown in Fig. 15 a) and b)

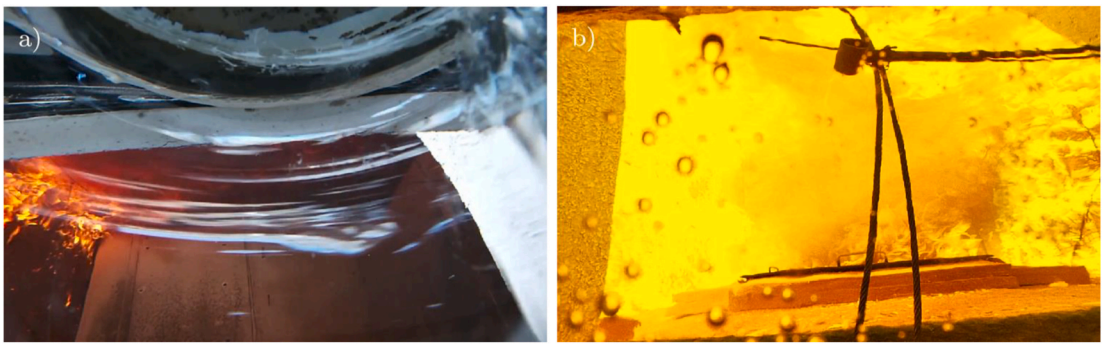

Fig. 13. Images showing interior of timber compartments after burn-out of kerosene. Subfigure a) shows only a limited area of flaming combustion near the top of the exposed side wall. Subfigure b) shows continued flaming combustion throughout the compartment.

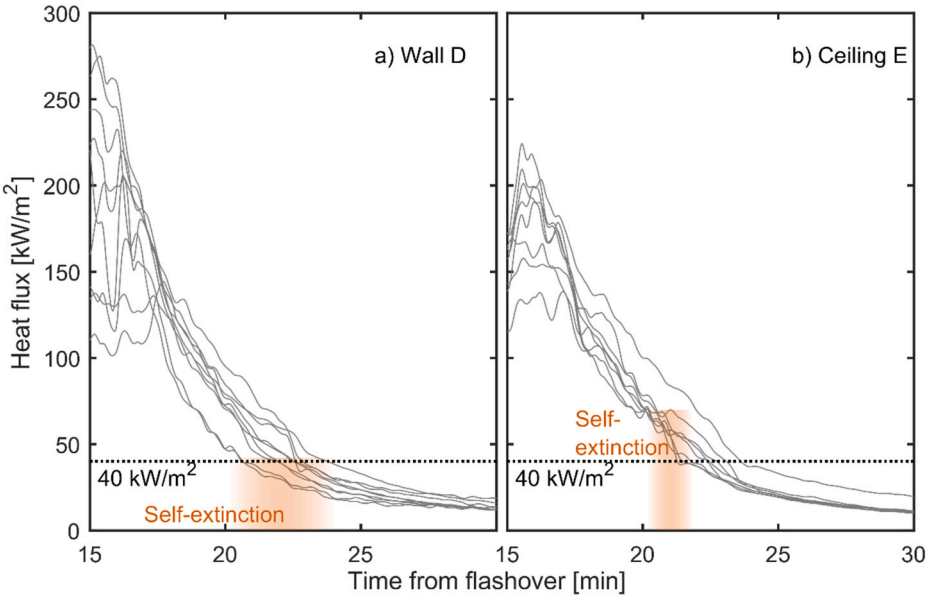

Fig. 14. Measured heat flux values for Test 2.2 with visually observed self-extinction range superimposed.

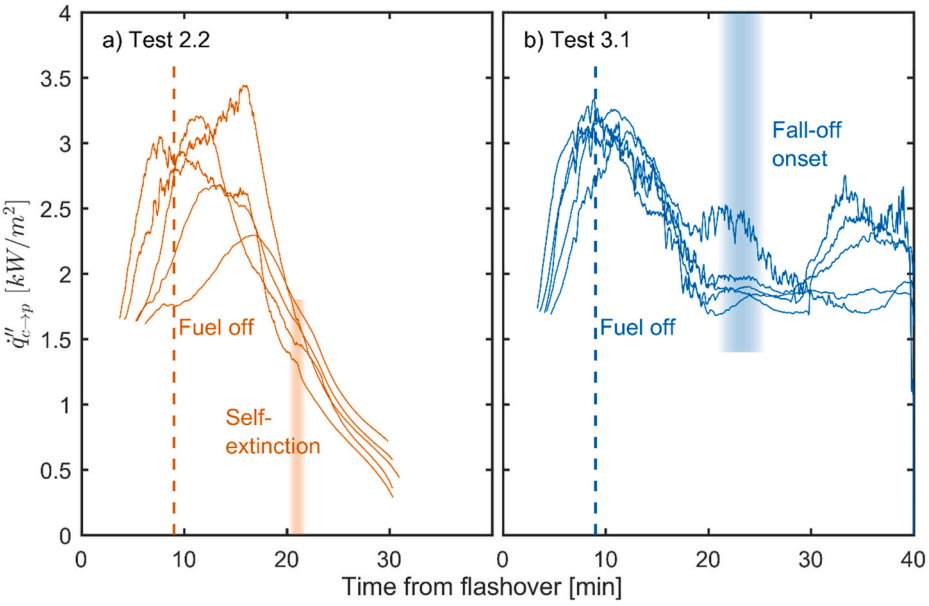

Fig. 15. In-depth temperature derived heat flux at the interface between char and pyrolysis regions for the ceiling in Test 2.2 and Test 3.1.

for tests 2.2 (two exposed surfaces) and 3.1 (three exposed surfaces), respectively. The heat flux values increased after ignition, reaching a peak around the time the fuel flow for the kerosene was closed, followed by continuous decay. Overall, the heat flux values in Test 3.1 appear to have been higher than those for Test 2.2, however, individual clusters in Test 2.2 showed the highest peak values. This aligns with the comparison of gas-phase temperatures and surface heat fluxes in each test, as these were generally higher for Test 3.1, but maximum values in certain locations were higher for Test 2.2 [14].

In Test 2.2, decay of the heat transfer continued alongside the decay of HRR (see Fig. 12) and incident heat flux (see Fig. 5) until self-extinction occurred at around 1.5 kW/m^2; in agreement with similar values previously reported by Emberley et al. [7]. For three exposed surfaces, the burnout of the kerosene fuel also led to a gradual drop in heat transfer from char to pyrolysis region, however, ultimately this reduction is arrested and a steady state heat transfer of approximately 1.75 kW/m^2 was established for about 10 min, before a renewed increase of conductive heat flux, which was linked to increased incident heat flux at the surface and loss of insulating char.

3.5. Fuel type study

The fuels studied here represent two distinct limits in mass transfer numbers [15,16] thus will have very different burning rates for equal heat feedback to the fuel surface. In reality, fuels likely consist of complex mixtures of plastic and cellulosic polymers with non-standard geometries and configurations. Some materials, for example timber, will form a carbon rich char, which will oxidize and smoulder at elevated temperatures, while some plastics will melt, pyrolyze and burn directly without leaving char residue.

In the context of compartment fires, long chain hydrocarbon fuels such as plastics, or in this case kerosene pools, possess larger mass

transfer (B-numbers) than wood cribs, meaning that the energy available to continually produce gaseous fuel is greater than the energy requirements to generate the gaseous fuel [14]. Wood cribs are distinct, as their porous physical structure shields most of the burning sticks from the external effects of the compartment, resulting in a reduced mass transfer number compared to pool fuels [16]; this resulted in a relatively longer burning duration for a wood crib compared to a pool fire with equivalent fuel load. Furthermore, the leftover smouldering char residue from the large quantity of burning wood created an additional radiation source that increases the thermal exposure onto the burning timber surfaces.

Considering these factors, Test 4.1 featured a compartment with two exposed surfaces ($A_e/A_T = 0.35$), with a wood crib fuel load that was adjusted to be identical to the Test 2.2 kerosene pool fire. Thus, a comparison of Test 2.2 and Test 4.1 enables a comparison of the effect of fuel type on the attainment of flaming self-extinction in the mass timber compartment.

The total HRR in tests 4.1 and 2.2, as measured from the buoyancy calorimeter are shown in Fig. 16 a). Fig. 16 b) shows the HRR of both the wood crib and pool fire. For the former, this was calculated from the measured mass loss of the crib with an assumed effective heat of combustion of 17.5 MJ/kg, and for the latter from the flow rate of kerosene with an assumed effective heat of combustion of 43.1 MJ/kg. The wood crib burned slower and therefore, despite its equal fuel load, extended the burning duration for Test 4.1 to a point where time-dependent mechanisms such as char fall-off occurred; despite this char fall-off occurring later than observed in Test 2.2 and Test 3.1. The smouldering wood crib residue and char fall-off are shown in Fig. 17.

After the occurrence of char fall-off, the total measured HRR in Test 4.1 increased from approximately 3.1 MW, 33 min after flashover, to approximately 4.4 MW, at 46 min after flashover (0.1 MW per minute). This rate of HRR increase was similar to that measured for Test 3.1, from 2 to 3.8 MW in 15 min (0.12 MW per minute). Despite the lower burning rate and HRR of the wood crib itself, the total HRRs during the fully-developed phase and onset of the decay phases were quite similar (within 500 kW, ~10 % of Test 2.2 steady HRR). There are two possibilities to explain the difference in moveable HRR: (1) the magnitude of heat fluxes and consequently burning rates of exposed timber is greater, and (2) more uniform heating in the compartment (both vertically and horizontally) resulting in a greater total mass of pyrolysates released. The first possibility can be considered from Fig. 5 which shows similar peak heat flux exposure to the exposed surfaces, however, for the encapsulated backwall the heat flux exposure was greater in Test 2.2. Preliminary analysis of the gas-phase temperature measurements from

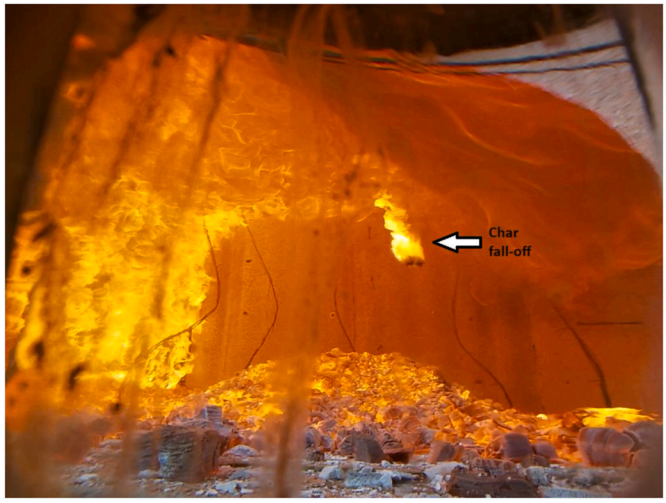

Fig. 17. Image showing collapsed wood crib in compartment. No flaming is visible from the charred remains of the wood crib but it is glowing visibly. Exposed timber side wall and ceiling are burning (flaming combustion). A piece of flaming timber/char can be seen falling from the ceiling and is labelled as 'Char fall-off'.

thermocouples during the fully-developed phase showed more uniform burning conditions and thermal exposures with the wood crib; this was described in a separate publication by Pope et al. [13]. This was associated with the aerodynamic stalling of the inflow air by the crib structure, resulting in a completely buoyancy-driven fire plume. As the crib was slowly consumed and collapsed, a large quantity of smouldering char from the crib residue formed, providing an additional heat source into the compartment [13].

4. Discussion

This section focuses on identifying relevant design considerations for the development of the self-extinction framework and associated tools for the adequate quantification of the mechanisms controlling the occurrence of self-extinction. These design considerations are related to the characteristic times.

In the case of encapsulated surfaces, the tools available for designers to prevent encapsulation failure must quantify its characteristic time for failure, $t_{f,e}$. The failure of plasterboard is complex and dependent on its composition and thickness itself, but also the mechanical fixings used to

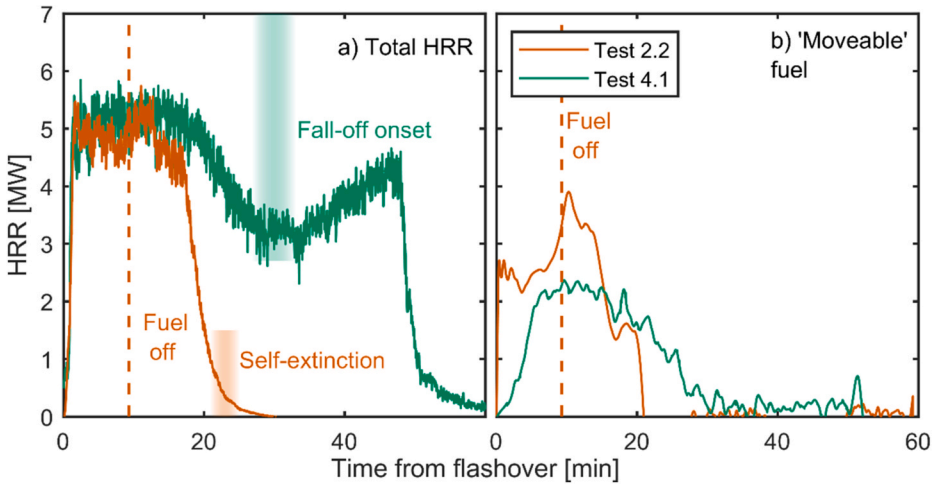

Fig. 16. Measurements of a) the total HRR and b) internal moveable fuel load HRR, for short pool fire fuelled Test 2.2 and wood crib fuelled Test 4.1, both with two surfaces exposed.

attach it to the timber surface. Proprietary fire ratings are available for most plasterboards; however, these are usually derived from standardised fire tests and thus do not reflect real time conditions in a compartment fire but exposure duration in a furnace following a standardised temperature time curve.

A surrogate for $t_{f,e}$ can be a critical failure temperature, nevertheless, this temperature needs to be treated with caution. For the conditions of these specific experiments, the onset of plasterboard failure was closely associated with the exceedance of 105 °C, herein considered as the completion of the drying process. Thus, the dehydration of the plasterboard can be considered a potential design target.

A second characteristic time scale is the time to char fall-off ($t_{f,c}$) and, under the presented experimental conditions, it was dominated by the thermal conditions at the first glue line interface. Once again, a surrogate temperature can be used. Nevertheless, the relationship between char fall-off and temperature was not as clear. In Test 2.1., when temperatures exceeded 100 °C at the first glue-line, what followed was a rapid temperature increase associated with char fall-off. However, in Test 2.2, thermocouples were observed to exceed 100 °C without char fall-off. In this case, no sudden temperature increase was observed, indicating that the 100°C threshold corresponded to the progression of the drying front. The results also show that, where fall-off did occur, the exceedance of 95 and 105 °C occurred in a relatively narrow time frame, compared to the failure of plasterboard. Therefore, the exceedance of 100 °C is not a suitable char fall-off indicator on its own but must be considered with additional information. The evidence provided here shows that 300 °C is not a suitable threshold since a rapid increase in temperature at the exceedance of 100 °C indicated char fall-off. Ultimately, char fall-off remains a complex phenomenon that depends not only on heat exposure but also on the type of adhesive, applied load and thermo-mechanical behaviour [29,35,43–45], thus simple temperature thresholds are unlikely to properly characterize $t_{f,c}$.

The characteristics of the fuel load will significantly affect both $t_{f,c}$ and $t_{f,e}$. The experimental data showed that the heat flux to all surfaces for the wood crib test was delayed, compared to the kerosene fire, despite achieving a similar peak total HRR. The kerosene resulted in a sootier fire, causing higher initial radiative heat flux values from the gas phase, compared to the wood crib. Nevertheless, the reduced burning rate of the fuel for the crib, paired with the radiation from the smouldering crib char residue also meant that the time to self-extinction was prolonged. Thus, the nature of the fuel has a significant influence on the relationship between the time to burn-out and the time for char fall-off. The fuel load used here was relatively low and below usual office or residential expected fuel loads. For real furniture the fuel will likely consists of a mix of fuel types, somewhere between the extreme conditions presented here of either pure cellulosic or pure hydrocarbon fuels.

Design must also account for the thermal feedback to the exposed timber surfaces from the other surfaces of the compartment. A critical thermal feedback condition can be achieved when more than a critical surface area of timber is exposed. When the exposed surface area is greater that this critical value the exposed timber walls and ceiling will continue to burn. Herein the influence of the ratio of exposed timber area to the total internal compartment area was qualified in observations of self-extinction and quantified in form of three parameters: the heat release rate, the incident heat fluxes on the surfaces of the exposed timber, and the net heat fluxes at the interface of char and timber.

The effect of exposure ratio is initially manifested during the decay of heat release and net heat flux after the burnout of the movable fuel load. Consistently with observations by Gorska [17], the rate of decay is inversely proportional to A_e/A_T and therefore, during decay, the attainment of equivalent thermal conditions is expected to be delayed with a higher exposure ratio.

As surfaces start to extinguish, the thermal decay within the compartment continues, ultimately resulting in flaming self-extinction of all exposed timber surfaces. In contrast, tests above the critical exposure condition showed that the decay of heat release and net heat flux in reached a steady state, thus suggesting that a thermal equilibrium point was attained in the compartment causing the continuous burning of timber. It cannot be clearly deduced if self-extinction can occur if char falls off, as in all cases studied, the onset of char fall-off occurred during periods when HRR was already decaying. However, the heat flux exposure values to all surfaces, and especially to the exposed surfaces indicate that this would have been unlikely as the median heat flux exposure did not fall below 170 kW/m^2.

After complete burnout of the movable fuel load, the incident heat measured at the surface of the exposed timber surfaces is the result of local incident heat flux from the flame attached to the timber surface and the radiative heat exchange within the compartment, which includes the burning timber surfaces, the encapsulated surfaces, the smoke layer and the opening. While during the thermal decay the smoke layer is shown to reduce in height, the role of the smoke layer appears to remain important. Therefore, a thermal feedback analysis solely based on a radiative feedback analysis between surfaces in an optically thin medium may not be sufficient, and the contribution from the smoke layer must be considered. The nature of the fuel residue is relevant since charring fuels can result in a large amount of oxidising charcoal on the floor after flameout of the movable fuel, which cannot be neglected from a radiative heat feedback point of view.

This series of experiments has unfortunately not been able to explore the effect of the ventilation factor on the occurrence of flaming self-extinction. Since the opening plays a major role controlling the heat losses in the compartment, the ratio of exposure to sustain critical conditions cannot be generalised to a specific area of exposed timber versus total compartment internal surface area.

5. Conclusions

This work describes outcomes from a series of compartment fire tests for full-scale timber compartments with a fixed opening and varying fuel types, fuel loads, and areas of timber exposure. Measurements are presented for the heat release rate, the temperatures at critical in-depth locations, namely the interface between timber and fire-rated plasterboard, and the first glue line, as well as heat flux measurements on all surfaces of the tested compartments and temperature gradient derived net heat flux measurements at the char-timber interface.

The experimental set-up allowed for careful control of the fuel load and, therefore, a clear distinction between burnout, defined as the cessation of flaming of the moveable fuel load, and self-extinction, defined as the cessation of flaming of combustible structural elements, i.e. timber. With the proliferation of tall buildings with exposed mass timber, a clear distinction between burnout and self-extinction should be considered critical for the fire safety strategy.

Flaming self-extinction was successfully achieved in a targeted test with a limited fuel duration that led to fuel burnout and self-extinction of two exposed timber surfaces (ceiling and wall) before char fall-off occurred. In a comparative test with a longer fuel duration, char fall-off occurred after approximately 22 min. This provided valuable reference data on the time to fall-off, which should be considered as a key design criterion for holistic fire safety engineering of engineered timber structures.

Self-extinction for an exposed wall aligned closely with a bench-scale heat flux threshold of 40 kW/m^2 for the specific timber used, however, self-extinction of the exposed ceiling occurred at higher measured heat flux values, around 70 kW/m^2.

Measured incident heat fluxes in the compartment were highest on exposed timber surfaces, and this effect was especially prominent after the original fuel load had burned out, causing a shift in fire dynamics from the centrally positioned moveable fuel load to the burning exposed timber surfaces.

Failure to achieve self-extinction was caused either through excessively high thermal feedback caused by too many exposed timber

surfaces, or by the occurrence of char fall-off when the burning duration was extended. The former was demonstrated for three exposed timber surfaces, which resulted in a steady state heat transfer from the char to the pyrolyzing timber greater than an extinction threshold. Char fall-off occurred in all tests that did not self-extinguish; it was especially prominent for a wood crib test, which was designed with the same fuel load and exposed timber as the pool fire test that did extinguish. As the wood crib burned out slower and its char provided additional heat flux, it prolonged critical heat flux values above self-extinction to the point of char fall-off. This highlighted the importance of the fuel type and should open conversations on the difference between charring and non-charring fuels and their effect on the overall heat balance in a mass timber compartment.

CRediT authorship contribution statement

Felix Wiesner: Writing – original draft, Visualization, Supervision, Investigation, Formal analysis, Data curation. **Hangyu Xu:** Writing – original draft, Visualization, Methodology, Formal analysis, Data curation. **David Lange:** Writing – review & editing, Conceptualization. **Vinny Gupta:** Writing – review & editing, Methodology, Investigation, Formal analysis, Data curation. **Ian Pope:** Writing – review & editing, Methodology, Investigation, Data curation. **José L. Torero:** Writing – review & editing, Funding acquisition, Conceptualization. **Juan P. Hidalgo:** Writing – review & editing, Supervision, Project administration, Methodology, Investigation, Funding acquisition, Formal analysis, Conceptualization.

Declaration of competing interest

The authors declare the following financial interests/personal relationships which may be considered as potential competing interests: Juan P. Hidalgo reports equipment, drugs, or supplies was provided by Queensland Fire and Emergency Services. Juan P. Hidalgo reports equipment, drugs, or supplies was provided by XLam. Juan P. Hidalgo reports equipment, drugs, or supplies was provided by Hyne Timber. Juan P. Hidalgo reports equipment, drugs, or supplies was provided by Lendlease. Juan P. Hidalgo reports equipment, drugs, or supplies was provided by Knauf. Juan P. Hidalgo reports equipment, drugs, or supplies was provided by Rockwool International. Editorial board member of the journal (Fire Safety Journal) - Felix Wiesner. Editorial board member of the journal (Fire Safety Journal) - David Lange. Editorial board member of the journal (Fire Safety Journal) - Juan P. Hidalgo. If there are other authors, they declare that they have no known competing financial interests or personal relationships that could have appeared to influence the work reported in this paper.

Acknowledgements

This project was funded by the ARC Future Timber Hub (IH150100030) and received generous support from QFES, XLam, Hyne Timber, Lend Lease, Knauf and Rockwool International A/S. The authors are extremely grateful to QFES for providing their research facility and engagement with the project. Dr Wiesner was supported by the National Centre for Timber Durability and Design Life. The authors are also thankful for technical guidance for the calorimeter design from Nathan White (CSIRO). Staff and students helping with the project are gratefully acknowledged: A. Bolanos, A. Browning, J. Cadena, E. Candansayar, P. Chowdhury, J. Carrascal, J. Cuevas, C. Gorska, M. Griffith, M. Hewitt, T. Iturralde, M. Javidnejad, G. Kanellopoulos, A. Lucherini, C. Maluk, S. Matthews, M. McLaggan, J. Mendez, A. Osorio, L. Ramadhan, A. Solarte, D. Soriguer, D. Tanudirdjo, W. Wu, H. Wyn, YH. Zhang, A. Zaben, and YS. Zhu.

Appendix A. Supplementary data

Supplementary data to this article can be found online at https://doi.org/10.1016/j.firesaf.2025.104346.

Data availability

Data will be made available via the UQ Library

References

[1] G. Churkina, A. Organschi, C.P.O. Reyer, A. Ruff, K. Vinke, Z. Liu, B.K. Reck, T. E. Graedel, H.J. Schellnhuber, Buildings as a global carbon sink, Nat. Sustain. (2020), https://doi.org/10.1038/s41893-019-0462-4.
[2] R. Brandner, G. Flatscher, A. Ringhofer, G. Schickhofer, A. Thiel, Cross laminated timber (CLT): overview and development, European J. Wood Wood Prod. 74 (2016) 331–351, https://doi.org/10.1007/s00107-015-0999-5.
[3] R.M. Hadden, A.I. Bartlett, J.P. Hidalgo, S. Santamaria, F. Wiesner, L.A. Bisby, S. Deeny, B. Lane, Effects of exposed cross laminated timber on compartment fire dynamics, Fire Saf. J. 91 (2017) 480–489, https://doi.org/10.1016/j.firesaf.2017.03.074.
[4] H. Xu, I. Pope, V. Gupta, J. Cadena, J. Carrascal, D. Lange, M.S. McLaggan, J. Mendez, A. Osorio, A. Solarte, D. Soriguer, J.L. Torero, F. Wiesner, A. Zaben, J. P. Hidalgo, Large-scale compartment fires to develop a self-extinction design framework for mass timber—Part 1: literature review and methodology, Fire Saf. J. 128 (2022) 103523, https://doi.org/10.1016/j.firesaf.2022.103523.
[5] R. Crielaard, J.-W. van de Kuilen, K. Terwel, G. Ravenshorst, P. Steenbakkers, Self-extinguishment of cross-laminated timber, Fire Saf. J. 105 (2019) 244–260, https://doi.org/10.1016/j.firesaf.2019.01.008.
[6] J. Cuevas Rodriguez, Critical Conditions for the Self-Extinction of Timber, PhD Thesis, The University of Queensland, 2022, https://doi.org/10.14264/d1405b5.
[7] R. Emberley, A. Inghelbrecht, Z. Yu, J.L. Torero, Self-extinction of Timber, Proceedings of the Combustion Institute, 2016, https://doi.org/10.1016/j.proci.2016.07.077.
[8] D. Morrisset, R.M. Hadden, A.I. Bartlett, A. Law, R. Emberley, Time dependent contribution of char oxidation and flame heat feedback on the mass loss rate of timber, Fire Saf. J. 120 (2021) 103058, https://doi.org/10.1016/j.firesaf.2020.103058.
[9] C.E. MacLeod, A. Law, R.M. Hadden, Quantifying the heat release from char oxidation in timber, Fire Saf. J. 138 (2023) 103793, https://doi.org/10.1016/j.firesaf.2023.103793.
[10] H. Mitchell, R. Amin, M. Heidari, P. Kotsovinos, G. Rein, Structural hazards of smouldering fires in timber buildings, Fire Saf. J. 140 (2023) 103861, https://doi.org/10.1016/j.firesaf.2023.103861.
[11] F. Wiesner, A. Bartlett, S. Mohaine, F. Robert, R. McNamee, J.-C. Mindeguia, L. Bisby, Structural Capacity of One-Way Spanning Large-Scale Cross-Laminated Timber Slabs in Standard and Natural Fires, Fire Technology, 2020, https://doi.org/10.1007/s10694-020-01003-y.
[12] T. Gernay, J. Zehfuß, S. Brunkhorst, F. Robert, P. Bamonte, R. McNamee, S. Mohaine, J.-M. Franssen, Experimental investigation of structural failure during the cooling phase of a fire: timber columns, Fire Mater. 47 (2023) 445–460, https://doi.org/10.1002/fam.3110.
[13] I. Pope, H. Xu, V. Gupta, J. Carrascal, D. Lange, M.S. McLaggan, J. Mendez Alvarez, A. Solarte, D. Soriguer, J.L. Torero, F. Wiesner, J.P. Hidalgo, in: C. Maluk, D. Lange, K.H. Tan, D. Zhang, Y. Zhang, J. Mendez Alvarez, A. Zaben, W. Wu, H. Xu, J. P. Hidalgo, F. Wiesner, M.S. McLaggan (Eds.), Fire Dynamics in Under-ventilated Mass Timber Room Compartments, The University of Queensland, Online, 2021.
[14] I. Pope, V. Gupta, H. Xu, F. Wiesner, D. Lange, J.L. Torero, J.P. Hidalgo, Fully-developed compartment fire dynamics in large-scale mass timber compartments, Fire Saf. J. 141 (2023) 104022, https://doi.org/10.1016/j.firesaf.2023.104022.
[15] T.Z. Harmathy, Effect of the nature of fuel on the characteristics of fully developed compartment fires, Fire Mater. 3 (1979) 49–60, https://doi.org/10.1002/fam.810030109.
[16] V. Gupta, J.L. Torero, J.P. Hidalgo, Burning dynamics and in-depth flame spread of wood cribs in large compartment fires, Combust. Flame 228 (2021) 42–56, https://doi.org/10.1016/j.combustflame.2021.01.031.
[17] C. Gorska Putynska, Fire Dynamics in Multi-Scale Timber Compartments, The University of Queensland, 2020.
[18] A. Lucherini, D.Š. Pitelková, V. Mózer, Estimating the effective char depth in structural timber elements exposed to natural fires, considering the heating and cooling phase, Eng. Struct. 323 (2025) 119255, https://doi.org/10.1016/j.engstruct.2024.119255.
[19] N. White, H. Xu, J. Abraham, J. Carrascal, J.P. Hidalgo, V. Gupta, N. Weerakkody, Buoyancy-driven Calorimeter for Post-flashover Heat Release Rate Measurements, University of Queensland, Brisbane, QLD, Australia, 2021.
[20] J.P. Hidalgo, C. Maluk, A. Cowlard, C. Abecassis-Empis, M. Krajcovic, J.L. Torero, A Thin Skin Calorimeter (TSC) for quantifying irradiation during large-scale fire testing, Int. J. Therm. Sci. 112 (2AD) 383–394. https://doi.org/10.1016/j.ijthermalsci.2016.10.013.
[21] N. Tondini, J.-M. Franssen, Analysis of experimental hydrocarbon localised fires with and without engulfed steel members, Fire Saf. J. 92 (2017) 9–22, https://doi.org/10.1016/j.firesaf.2017.05.011.

[22] C. Gorska, J.P. Hidalgo, J.L. Torero, Fire dynamics in mass timber compartments, Fire Saf. J. 120 (2021) 103098, https://doi.org/10.1016/j.firesaf.2020.103098.
[23] CEN, Eurocode 1: Actions on structures - Part 1-2: General actions - Actions on structures exposed to fire, EN 1991-1-2:2002, in: , 2002.
[24] J. Su, P.S. Lafrance, M.S. Hoehler, M.F. Bundy, Fire Safety Challenges of Tall Wood Buildings–phase 2: Task 3-Cross Laminated Timber Compartment Fire Tests, NIST, Gaithersburg, USA, 2018.
[25] X. Li, X. Zhang, G. Hadjisophocleous, C. McGregor, Experimental study of combustible and non-combustible construction in a natural fire, Fire Technol. 51 (2014) 1447–1474, https://doi.org/10.1007/s10694-014-0407-4.
[26] D.I. Kolaitis, M.A. Founti, Development of a solid reaction kinetics gypsum dehydration model appropriate for CFD simulation of gypsum plasterboard wall assemblies exposed to fire, Fire Saf. J. 58 (2013) 151–159, https://doi.org/10.1016/j.firesaf.2013.01.029.
[27] M. Violette, Memoire sur les Charbons de Bois, Ann. Chem. Phys. 32 (1851) 304.
[28] C. Di Blasi, Modeling chemical and physical processes of wood and biomass pyrolysis, Prog. Energy Combust. Sci. 34 (2008) 47–90, https://doi.org/10.1016/j.pecs.2006.12.001.
[29] A. Čolić, F. Wiesner, L. Bisby, J.P. Hidalgo, Delamination and Char Fall-Off in Fire-Exposed Cross-Laminated Timber Loaded in Shear, University of Queensland, Brisbane, QLD, Australia, 2021, https://doi.org/10.14264/a067f63.
[30] A. Law, R.M. Hadden, Burnout means burnout. SFPE Europe Magazine, 2017.
[31] C. McGregor, Contribution of cross laminated timber panels to room fires, Master's Thesis, Carleton University, 2013. https://doi.org/10.22215/etd/2013-06885.
[32] F. Wiesner, S. Deeny, L.A. Bisby, Influence of ply configuration and adhesive type on cross-laminated timber in flexure at elevated temperatures, Fire Saf. J. 120 (2021) 103073, https://doi.org/10.1016/j.firesaf.2020.103073.
[33] S.L. Zelinka, K. Sullivan, S. Pei, N. Ottum, N.J. Bechle, D.R. Rammer, L. E. Hasburgh, Small scale tests on the performance of adhesives used in cross laminated timber (CLT) at elevated temperatures, Int. J. Adhesion Adhes. 95 (2019) 102436, https://doi.org/10.1016/j.ijadhadh.2019.102436.
[34] R. Zhang, H. Dai, G.D. Smith, Investigation of the high temperature performance of a polyurethane adhesive used for structural wood composites, Int. J. Adhesion Adhes. (2021) 102882, https://doi.org/10.1016/j.ijadhadh.2021.102882.
[35] M. Cheung, A. Zaben, C. Maluk, Experimental method for studying the effects of elevated temperature in adhesives used in laminated Mass Timber, Fire Saf. J. 146 (2024) 104058, https://doi.org/10.1016/j.firesaf.2023.104058.
[36] A. Čolić, F. Wiesner, D. Hopkin, M. Spearpoint, W. Wu, L. Bisby, Application of microscale methods to study the heat-induced delamination in engineered wood products bonded with one-component polyurethane adhesives, Int. J. Adhesion Adhes. 135 (2024) 103834, https://doi.org/10.1016/j.ijadhadh.2024.103834.
[37] R. Emberley, T. Do, J. Yim, J.L. Torero, Critical heat flux and mass loss rate for extinction of flaming combustion of timber, Fire Saf. J. (2017), https://doi.org/10.1016/j.firesaf.2017.03.008.
[38] J. Hietaniemi, E. Mikkola, Design Fires for Fire Safety Engineering, VTT Working Papers 139, VTT Technical Research Centre of Finland, 2010.
[39] J. Cuevas, J.L. Torero, C. Maluk, Flame extinction and burning behaviour of timber under varied oxygen concentrations, Fire Saf. J. 120 (2021) 103087, https://doi.org/10.1016/j.firesaf.2020.103087.
[40] D. Hopkin, W. Węgrzyński, C. Gorska, M. Spearpoint, J. Bielawski, H. Krenn, T. Sleik, R. Blondeau, G. Stapf, Full-scale fire experiments on cross-laminated timber residential enclosures featuring different lining protection configurations, Fire Technol. 60 (2024) 3771–3803, https://doi.org/10.1007/s10694-024-01581-1.
[41] F. Wiesner, R. Hadden, L. Bisby, in: D. Lange, C. Maluk, K.H. Tan, D. Zhang, Y. Zhang, J. Mendez Alvarez, A. Zaben, W. Wu, H. Xu, J.P. Hidalgo, F. Wiesner, M. S. McLaggan (Eds.), Influence of Adhesive on Decay Phase Temperature Profile in CLT in Fire, The University of Queensland, Online, 2021.
[42] CEN, Eurocode 5: Design of timber structures. Part 1-2: Generalstructure fire design, EN 1995-1-2:2004, in: , 2009.
[43] E. Johansson, A. Svenningsson, Delamination of cross-laminated timber and its impact on fire development - Focusing on different types of adhesives, Lund University, 2018. Report 5562.
[44] C. Dagenais, L. Ranger, Revisiting heat delamination characteristics of adhesives in cross-laminated timber, in: Seoul, South Korea, 2018.
[45] A.A.A. Awadallaha, R. Hadden, A. Law, Meta-analysis of temperature, heat release rate, delamination and auto-extinction of timber compartments, Fire Saf. J. 146 (2024), https://doi.org/10.1016/j.firesaf.2024.104164.